Secretory cargo sorting by Ca^{2+}-dependent Cab45 oligomerization at the trans-Golgi network

Alvaro H. Crevenna,[1]* Birgit Blank,[2]* Andreas Maiser,[3,4] Derya Emin,[1] Jens Prescher,[1] Gisela Beck,[2] Christine Kienzle,[2] Kira Bartnik,[1] Bianca Habermann,[2] Mehrshad Pakdel,[2] Heinrich Leonhardt,[3,4] Don C. Lamb,[1] and Julia von Blume[2]

[1]Physical Chemistry, Department of Chemistry Center for Nanoscience, Nanosystems Initiative Munich and Center for Integrated Protein Science Munich, Ludwig Maximilians University Munich, 81377 Munich, Germany
[2]Max Planck Institute of Biochemistry, 82152 Martinsried, Germany
[3]Department of Biology II and [4]Center for Integrated Protein Science, Ludwig Maximilians University Munich, 82152 Martinsried, Germany

Sorting and export of transmembrane cargoes and lysosomal hydrolases at the trans-Golgi network (TGN) are well understood. However, elucidation of the mechanism by which secretory cargoes are segregated for their release into the extracellular space remains a challenge. We have previously demonstrated that, in a reaction that requires Ca^{2+}, the soluble TGN-resident protein Cab45 is necessary for the sorting of secretory cargoes at the TGN. Here, we report that Cab45 reversibly assembles into oligomers in the presence of Ca^{2+}. These Cab45 oligomers specifically bind secretory proteins, such as COMP and LyzC, in a Ca^{2+}-dependent manner in vitro. In intact cells, mutation of the Ca^{2+}-binding sites in Cab45 impairs oligomerization, as well as COMP and LyzC sorting. Superresolution microscopy revealed that Cab45 colocalizes with secretory proteins and the TGN Ca^{2+} pump (SPCA1) in specific TGN microdomains. These findings reveal that Ca^{2+}-dependent changes in Cab45 mediate sorting of specific cargo molecules at the TGN.

Introduction

All newly synthesized secretory proteins arrive at the Golgi apparatus from the ER (Palade, 1975). In the very last subcompartment of the Golgi stack, which is generally referred to as the TGN, the diverse cargoes are sorted from each other and from the Golgi-resident proteins, packed into specific transport carriers, and exported to their respective destinations (De Matteis and Luini, 2008; Guo et al., 2014; Kienzle and von Blume, 2014). The sorting of lysosomal hydrolases is well understood (Kornfeld and Mellman, 1989; Traub and Kornfeld, 1997; Doray et al., 2002), as are the signals in the cytoplasmic domains of transmembrane cargoes that mediate their incorporation into clathrin-coated vesicles for their export from the TGN (Fölsch et al., 1999, 2001; Mellman and Nelson, 2008; Bonifacino, 2014). However, no cargo receptors for the sorting and packing of secretory proteins have been identified at the TGN.

In recent years, we have studied a novel and conserved cargo receptor–independent mechanism implicated in the sorting of secretory cargo at the TGN (von Blume et al., 2011; Curwin et al., 2012). In this process, F-actin and cofilin bind to, and activate, the TGN-specific Ca^{2+} pump SPCA1 (Lissandron et al., 2010; Kienzle et al., 2014), which results in an influx of Ca^{2+} into a specific domain of the TGN (von Blume et al., 2011). We suggested that this transient local increase in Ca^{2+} concentration involves Cab45, a protein that is required for secretory protein sorting and is normally retained in the TGN (Kienzle and von Blume, 2014). Here, we investigate how Ca^{2+} and Cab45 act together to sort secretory proteins at the TGN.

Results and discussion

Previous work has shown that soluble Ca^{2+}-binding ER- or sarcoplasmic reticulum–resident proteins form oligomers in the presence of Ca^{2+} (Meissner, 1975). Thus, we hypothesized that soluble Cab45 might oligomerize upon Ca^{2+} binding. To investigate the state of Cab45 in cells, we incubated purified Golgi membranes under control or Ca^{2+} depletion conditions, and subjected them to Blue NativePAGE gel electrophoresis, denaturing SDS-PAGE, and Western blotting (WB) with a Cab45 antibody. Under control conditions, Cab45 appears as low-(45 kD) and high molecular mass (1,000 kD) fractions (Fig. 1 A), but upon treatment of the membranes with the Ca^{2+} chelator BAPTA-AM, the latter fraction was not evident (Fig. 1 A). On the denaturing SDS-PAGE, Cab45 is detectable at a molecular mass of ∼50 kD and the Golgi preparation consists of a trans-Golgi compartment as visualized by the TGN46 Western blot.

*A.H. Crevenna and B. Blank contributed equally to this paper.

Correspondence to Julia von Blume: vonblume@biochem.mpg.de; or Alvaro H. Crevenna: alvaro.crevenna@cup.uni-muenchen.de

Abbreviations used in this paper: BB, breaking buffer; Cab45, Ca^{2+} binding protein 45 kD; CD, circular dichroism; dSTORM, direct stochastic optical reconstruction microscopy; EFh, EF hand; SIM, structural illumination microscopy; WB, Western blotting; WT, wild type.

The Rockefeller University Press $30.00
J. Cell Biol. Vol. 213 No. 3 305–314
www.jcb.org/cgi/doi/10.1083/jcb.201601089

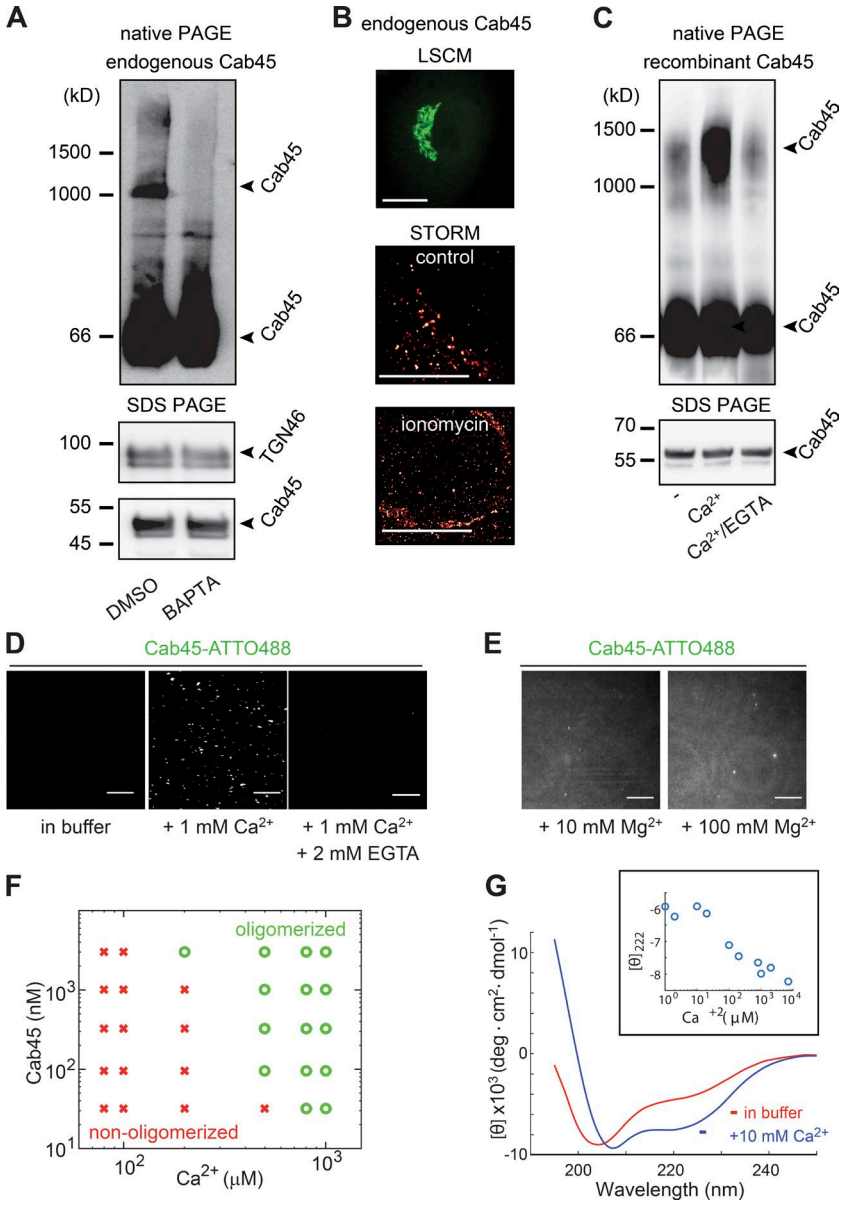

Figure 1. **Cab45 self-assembles in the presence of Ca^{2+}.** (A) Purified Golgi membranes from HeLa cells were incubated with DMSO (control) or 25 µM BAPTA-AM for 15 min at 37°C. Subsequently, membranes were lysed in NativePAGE buffer containing 1% DDM, subjected to NativePAGE (3–12%, top) or denaturing SDS-PAGE and analyzed by WB with TGN46 (middle) or anti-Cab45 (bottom) antibodies. (B) Top: HeLa cells were fixed and stained with a Cab45 and an Alexa Fluor 488–labeled antibody and analyzed by laser scanning confocal microscopy (LSCM). Bottom two panels: HeLa cells were incubated with a Ca^{2+}-containing buffer supplemented with DMSO (control) or a Ca^{2+}-free Hanks' buffer containing 2 µM ionomycin and 5 mM EGTA (Palmer and Tsien, 2006) for 10 min. Then, cells were fixed and stained with the Cab45 antibody and a secondary, Cy5-labeled antibody. dSTORM imaging was performed using widefield illumination and single fluorescent emitters were localized using a Gaussian least-squares fit. Bars, 10 µm. (C) Recombinant Cab45 was incubated in calcium-free buffer, with 1 mM Ca^{2+} or with 1 mM Ca^{2+} and 2 mM EGTA. Samples were subjected to NativePAGE (top) or SDS-PAGE (bottom) and analyzed by WB with an anti-Cab45 antibody. (D) Recombinant ATTO-488–labeled Cab45 was incubated as in (C) and analyzed by confocal microscopy. (E) Recombinant ATTO-488-labeled Cab45 was treated with 10 or 100 mM Mg^{2+} and analyzed by confocal microscopy. Bars, 20 µm (F) Oligomerization of Cab45 was assessed by fluorescence microscopy as a function of Ca^{2+} and protein concentration. (G) Far-UV CD analysis of recombinant Cab45 in the presence and absence of Ca^{2+}. (Inset) Ellipticity of Cab45 at 222 nm plotted as a function of Ca^{2+} concentration.

To visualize the effects of Ca^{2+} on Cab45 in cells, untreated or ionomycin-treated HeLa cells were fixed and stained with a Cab45 antibody and imaged by direct stochastic optical reconstruction microscopy (dSTORM; Heilemann et al., 2008). In control cells, Cab45 was detected in dense clusters (Fig. 1 B). In contrast, in cells treated with ionomycin (a Ca^{2+} ionophore) Cab45 appeared in much smaller and more diffuse punctae (Fig. 1 B) without an apparent effect on TGN morphology (Fig. S1 A). These findings suggest the existence of large, Ca^{2+}-dependent Cab45 protein complexes in cells.

To gain further insights into the change in Cab45 organization by Ca^{2+}, we switched to a reconstituted system. Recombinant Cab45 was incubated with Ca^{2+} or Ca^{2+}/EGTA or left untreated. Subsequent analysis by NativePAGE and WB of Cab45 incubated with Ca^{2+} alone revealed the presence of both high and low molecular mass fractions, whereas the former was much less prominent in both untreated and Ca^{2+}/EGTA-treated samples (Fig. 1 C). Next, we visualized ATTO488-labeled recombinant Cab45 with confocal microscopy. In the absence of Ca^{2+}, we did not observe Cab45 oligomers. The addition of 1 mM Ca^{2+} promoted the formation of fluorescent Cab45 oligomers (Fig. 1 D), and excess EGTA reversed this change (Fig. 1 D). Oligomerization was Ca^{2+} specific and was not affected by similar or higher concentration of Mg^{2+} (Fig. 1 E). Furthermore, in a double titration experiment, we observed that oligomerization depends more strongly on the Ca^{2+} concentration than on the Cab45 concentration (Fig. 1 F). In addition, measurements of the circular dichroism (CD) revealed a change in the secondary structure of Cab45 upon addition of Ca^{2+} (Fig. 1 G), with the largest shift in secondary structure content occurring between 100 and 200 µM Ca^{2+} (Fig. 1 G, inset). Analysis of the CD spectrum using CONTIN (Wiech et al., 1996) showed that the change reflected a decrease in β-sheet (from 0.31 to 0.23) with a concomitant increase in α-helicity (from 0.18 to 0.27) but no significant alteration in random coil content. Given that the concentration of Ca^{2+} at the TGN is believed to be ∼130 µM (Missiaen et al., 2004; Pizzo et al., 2011), the oligomer we observe likely represents the form of Cab45 physiologically found in the TGN of cells.

Cab45 is known to coprecipitate with secretory proteins from HeLa cell lysates such as COMP or LyzC (von Blume et

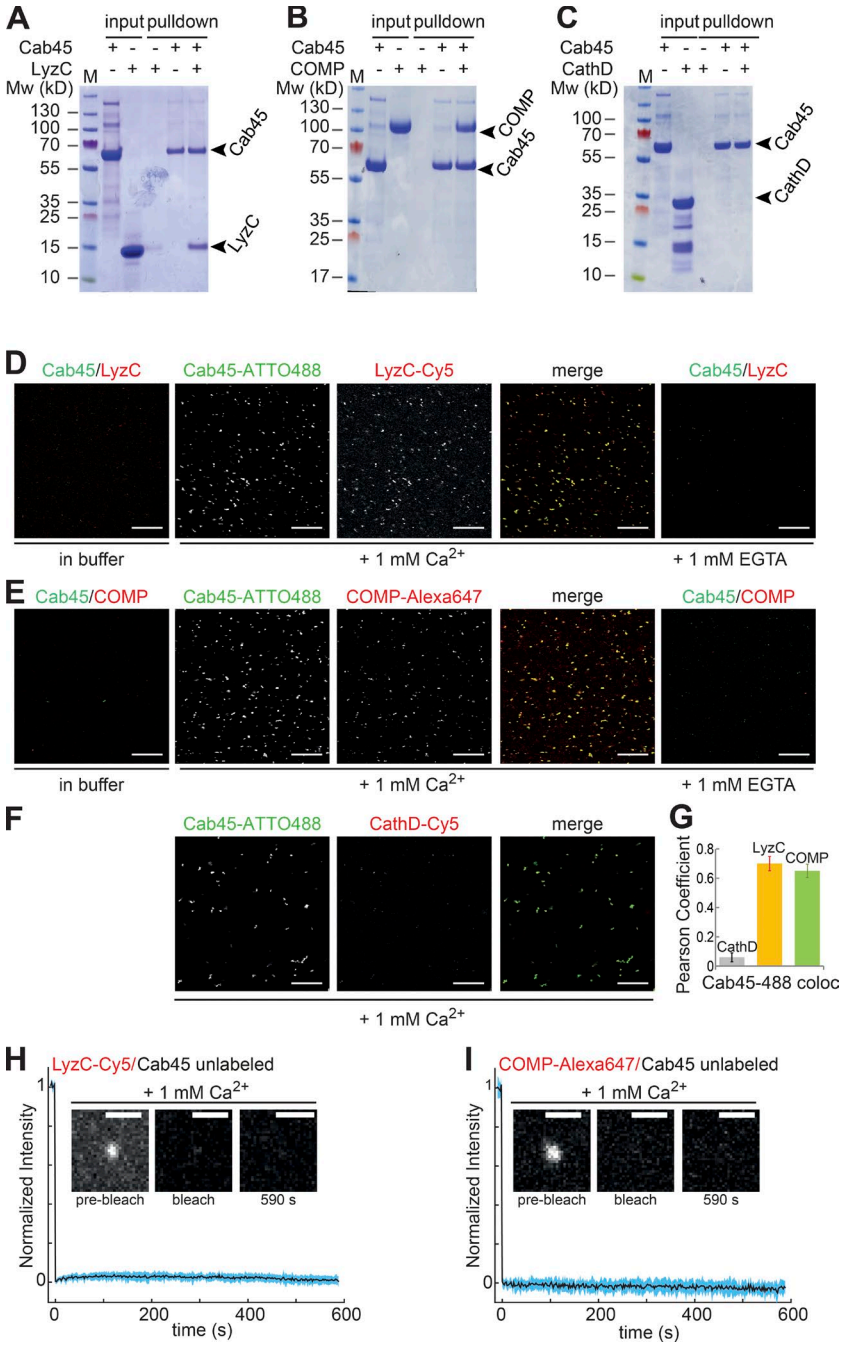

Figure 2. **Cargo recruitment by Cab45 oligomers.** (A–C) Pull-down experiments performed with His-tagged Cab45 and the potential cargo molecules LyzC (A), COMP (B), and CathepsinD (C), analyzed by SDS-PAGE and Coomassie staining. (D–F) In vitro oligomerization assay. Cab45 and LyzC (D), COMP (E) or CathepsinD (F), labeled as indicated, were incubated in Ca^{2+}-free buffer, with Ca^{2+} or Ca^{2+}/EGTA. Bars, 20 µm. (G) Pearson coefficient of colocalization between Cab45-ATTO488 and potential cargo molecules. Error bars represent SD from three independent experiments (n = 3). Two images were quantified per experiment. (H and I) FRAP analysis of LyzC-Cy5 (H) and COMP–Alexa Fluor 647 (I) recruited to individual unlabeled Cab45 oligomers. The black line is the mean signal, whereas the light blue trace represents one SD on either side (n = 13 for LyzC and 15 for COMP). The insets show examples of a Cab45 oligomer before bleaching (prebleach), immediately after bleaching (bleach), and ∼10 min after bleaching (590 s). Bar, 2 µm.

al., 2012). To determine whether the interaction is direct, we incubated recombinant His-tagged Cab45 attached to nickel nitrilotriacetic acid beads with recombinant LyzC, COMP or CathepsinD (a lysosomal hydrolase) in the presence of Ca^{2+} and performed pull-down experiments. SDS-PAGE analysis showed that both LyzC and COMP, but not CathepsinD, bound directly to Cab45 in the presence of Ca^{2+} (Fig. 2, A–C). Next, we wanted to explore whether cargo molecules are recruited specifically by Cab45 oligomers. To this end, we incubated recombinant ATTO488-labeled Cab45 with LyzC-Cy5, COMP–Alexa Fluor 647, or CathepsinD-Cy5 in the presence of Ca^{2+} or Ca^{2+}/EGTA, or under Ca^{2+}-free conditions, and analyzed the samples by confocal microscopy. Both LyzC and COMP were found to colocalize with Cab45 in the presence of Ca^{2+}, which suggested cargo recruitment to the oligomeric form (Fig. 2, D, E, and G; and Fig. S1, B and C). Colocalization was also reversible upon addition of EGTA (Fig. 2, D and E). Neither of the secretory proteins showed any detectable oligomerization in the absence of Cab45 (Fig. S1, B and C). CathepsinD did not interact with Cab45 at all (Fig. 2, F and G). Recruitment of cargo to Cab45 clusters appears to be stable, as there was no protein exchange within 10 min as assessed by FRAP (Fig. 2, H and I). Because Cab45 exists in at least two forms in the presence of Ca^{2+}, we wanted to know which form binds cargo. Hence, we incubated Cab45-ATTO488 with fluorescently labeled LyzC or COMP and performed fluorescence cross-correlation spectroscopy in the absence and presence of Ca^{2+}. We observed no cross-correlation between nonoligomerized Cab45 and either secretory protein in the absence or presence of 1 mM Ca^{2+} (Fig. S1, D and E). Thus, only the oligomer seems capable of recruiting

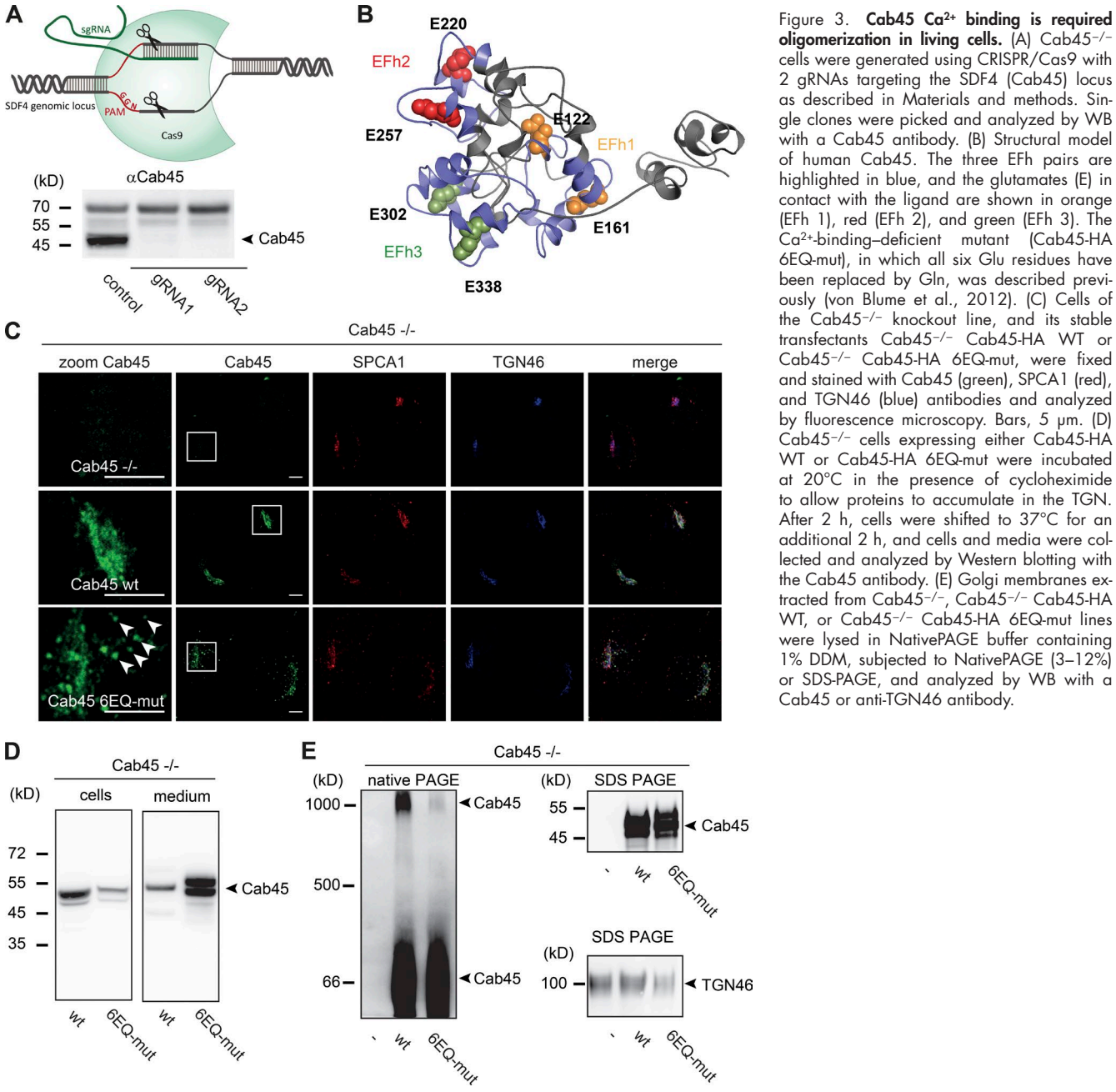

Figure 3. **Cab45 Ca^{2+} binding is required oligomerization in living cells.** (A) Cab45$^{-/-}$ cells were generated using CRISPR/Cas9 with 2 gRNAs targeting the SDF4 (Cab45) locus as described in Materials and methods. Single clones were picked and analyzed by WB with a Cab45 antibody. (B) Structural model of human Cab45. The three EFh pairs are highlighted in blue, and the glutamates (E) in contact with the ligand are shown in orange (EFh 1), red (EFh 2), and green (EFh 3). The Ca^{2+}-binding–deficient mutant (Cab45-HA 6EQ-mut), in which all six Glu residues have been replaced by Gln, was described previously (von Blume et al., 2012). (C) Cells of the Cab45$^{-/-}$ knockout line, and its stable transfectants Cab45$^{-/-}$ Cab45-HA WT or Cab45$^{-/-}$ Cab45-HA 6EQ-mut, were fixed and stained with Cab45 (green), SPCA1 (red), and TGN46 (blue) antibodies and analyzed by fluorescence microscopy. Bars, 5 µm. (D) Cab45$^{-/-}$ cells expressing either Cab45-HA WT or Cab45-HA 6EQ-mut were incubated at 20°C in the presence of cycloheximide to allow proteins to accumulate in the TGN. After 2 h, cells were shifted to 37°C for an additional 2 h, and cells and media were collected and analyzed by Western blotting with the Cab45 antibody. (E) Golgi membranes extracted from Cab45$^{-/-}$, Cab45$^{-/-}$ Cab45-HA WT, or Cab45$^{-/-}$ Cab45-HA 6EQ-mut lines were lysed in NativePAGE buffer containing 1% DDM, subjected to NativePAGE (3–12%) or SDS-PAGE, and analyzed by WB with a Cab45 or anti-TGN46 antibody.

secretory proteins (Fig. 2, D and E; and Fig. S1, D and E). Collectively, the data suggest that oligomeric Cab45 forms stable complexes with specific molecules, which can be released when reducing the Ca^{2+} concentration.

To further investigate the role of Cab45 during cargo sorting in living cells, we generated a Cab45 knockout HeLa cell line (Cab45$^{-/-}$) using CRISPR/Cas9 technology (Cong et al., 2013; Fig. 3 A and Fig. S2 A). To test for the effects on protein secretion, we transfected these cells with Flag-LyzC for 24 h or detected endogenous COMP directly. After 4-h incubation in serum-free medium, samples were collected, processed and analyzed by WB with specific antibodies and quantified (Fig. S2, B–E). Cab45$^{-/-}$ cells showed a significant reduction in secretion of COMP and LyzC (Fig. S2, B–E), similar to that seen in Cab45 siRNA lines (von Blume et al., 2012).

Cab45 has three consecutive EF hand (EFh) domains. A structural model of Cab45 was generated to visualize the arrangement of the three EFh domains in space (Fig. 3 B). Next, to investigate the role of its Ca^{2+} binding sites on Cab45-mediated sorting and secretion, we transduced Cab45$^{-/-}$ cells with Cab45-HA wild-type (WT) or Cab45-HA 6EQ-mut in which all Ca^{2+} binding sites have been mutated (Fig. 3 B). Although both proteins localized to the TGN as well as to SPCA1, Cab45 6EQ-mut was also observed in vesicles around the TGN, suggesting export of the normally TGN-resident protein (Fig. 3 C). To check this, Cab45 WT and Cab45 6EQ-mut cells were treated with cycloheximide and incubated at 20°C for 2 h to inhibit export from the TGN (von Blume et al., 2009). Cells were then shifted to 37°C to release the TGN-accumulated proteins, and cells and culture supernatant were analyzed by WB. Cab45 WT was predominantly found in the cell pellet (83%, $n = 3$), whereas a large proportion

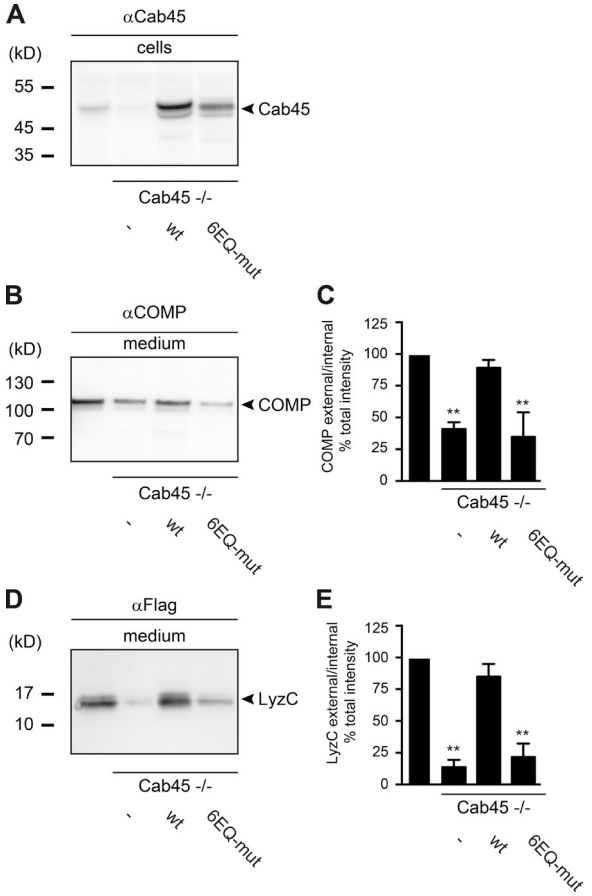

Figure 4. **Cab45 Ca^{2+} binding is required for sorting in living cells.** (A) Cell lysates of Cab45$^{-/-}$, Cab45$^{-/-}$ Cab45-HA WT or Cab45$^{-/-}$ Cab45-HA 6EQ-mut HeLa cells were analyzed by WB with a Cab45 antibody. (B and D) Cell culture supernatants of the same cells were incubated in serum-free medium for 4 h at 37°C. Media and cell extracts were blotted and probed with antibodies against COMP (B) or Flag (LyzC; D). Western blots from three independent experiments were quantified by densitometry using the ImageJ software. Bar graphs represent the densitometry values of external COMP (C) and LyzC (E) normalized to internal protein contents, respectively. Error bars represent SD calculated of three independent experiments of secreted COMP (C) or LyzC (E), respectively (n = 3). **, $P < 0.01$ (compared datasets).

of the Cab45 6EQ-mut was detected in the culture supernatant (94%, n = 3; Fig. 3 D). To test whether Ca^{2+}-dependent oligomerization was responsible for Cab45 secretion, Golgi membranes purified from Cab45$^{-/-}$, Cab45$^{-/-}$ Cab45-HA WT, or Cab45$^{-/-}$ Cab45-HA 6EQ-mut cells were analyzed by NativePAGE and WB. Like the endogenous protein (Fig. 1 A), Cab45-HA WT was detectable in low and high molecular mass forms, but the latter was missing from cells expressing Cab45 6EQ-mut (Fig. 3 E).

Finally, we assessed the role of these mutations in TGN sorting (Fig. 4). The expression level of Cab45 in control, Cab45$^{-/-}$, Cab45$^{-/-}$ WT, or 6EQ-mut HeLa cells was analyzed by WB (Fig. 4 A). In addition, supernatants from these cell cultures expressing Flag-LyzC were analyzed by WB (Fig. 4, B and D) and quantified (Fig. 4, C and E). Cab45 WT, but not the Cab45 6EQ-mut protein, rescued secretion of both LyzC and COMP (Fig. 4, B–E). These results thus demonstrate that Cab45 oligomerization in cells requires its Ca^{2+}-binding sites and that Ca^{2+}-dependent Cab45 oligomerization is necessary for sorting in living cells.

Given that Cab45 oligomerization is Ca^{2+} dependent, these oligomers might form in the vicinity of SPCA1. To investigate the distribution of Cab45, SPCA1, and cargo (LyzC) in intact cells, we used 3D structural illumination microscopy (SIM; Schermelleh et al., 2010; Cardoso et al., 2012). HeLa cells stably expressing HA-SPCA1 were fixed and stained with antibodies specific for Cab45 and HA (SPCA1: Fig. 5 A and Fig. S3, A–C; Flag LyzC: Fig. 5 B and Fig. S3, D–F; p230 [a TGN resident]: Fig. 5 C and Fig. S3, G–I; or TGN46: Fig. 5 D and Fig. S3, J–L, antibodies, respectively). The analysis revealed that ∼60% and 30% Cab45 colocalized, in small clusters with SPCA1 and LyzC, respectively (Fig. 5 E). In contrast, only 10% of p230 and 18% of TGN46 colocalized with Cab45 (Fig. 5 E). These results suggest that oligomerized Cab45 may preferentially accumulate near SPCA1 to segregate cargo. The close proximity between these components may suggest the formation of a functional sorting module regulated by Ca^{2+}. The inhomogeneous distribution of Cab45 observed at the TGN may be related to two recently postulated TGN sub-compartments, trans-Golgi compartment1 (tGo1) and tGo2 (Aulestia et al., 2015). In particular, Cab45 may be present only at the tGo1, the compartment in which SPCA1 is active (Aulestia et al., 2015).

In summary, our results suggest the following mechanism for Cab45-mediated sorting at the TGN. Upon SPCA1-mediated Ca^{2+} influx into the lumen, Cab45 binds Ca^{2+}, triggering a conformational change and allowing oligomerization. Cab45 oligomers then bind specific proteins, thereby sorting cargo from noncargo (Fig. 5 F). We propose to refer to this Cab45 sorting oligomer as a cernosome, from the Latin *cernere*, which means to choose, sift, separate, decide, or distinguish. The required dissociation of the Cab45 cargo complex (because Cab45 is not packed into transport carriers) may then occur either by reduction of free calcium levels or via a signal such as phosphorylation by a Golgi kinase (e.g., Golgi casein kinase Fam20C; Tagliabracci et al., 2012). The cernosome represents an elegant means of segregating different cargoes by recognition of the Cab45 oligomer. This is therefore a unique way to export cargo independent of a bona fide cargo receptor.

Materials and methods

Antibodies, plasmids, and cell culture

The commercial antibodies used in this study, and their sources, are as follows: Anti-COMP (rabbit polyclonal, ab74524; Abcam), anti-FLAG (mouse monoclonal, F3165; Sigma-Aldrich), and anti-TGN46 (sheep polyclonal, AHP500G; AbD Serotec) were used for WB, together with the secondary antibodies sheep (sc-2770, sc-2303, rabbit sc-2301 and mouse sc-2314) obtained from Santa Cruz Biotechnology, Inc. Anti-HA (rat monoclonal, 11867423001; Roche), anti-FLAG (mouse monoclonal; F3165; Sigma-Aldrich), anti-GM130 (mouse monoclonal, 610822; BD Biosciences), and anti-ATP2C1 (mouse monoclonal, HPA035116; Sigma-Aldrich) were used for immunofluorescence microscopy. The secondary antibodies Alexa Fluor 488 rabbit (A21206), Alexa Fluor 594 mouse (A21203), and Alexa Fluor 488 rat (A21208) were purchased from Thermo Fisher Scientific. For STORM measurements Cy5-conjugated AffiniPure (rabbit, 711–175-152; Jackson ImmunoResearch Laboratories, Inc.) was used for Cab45 as a secondary antibody and Alexa Fluor 488 sheep (A11015) for TGN46 (Thermo Fisher Scientific). The recombinant proteins COMP-FLAG (COMP-3659H; Creative BioMart), COMP (ab104358; Abcam), LysozymeC (Sigma-Aldrich), and LysozymeC-Cy5 (LS1-S5-1; Nanocs) were used for in vitro analysis.

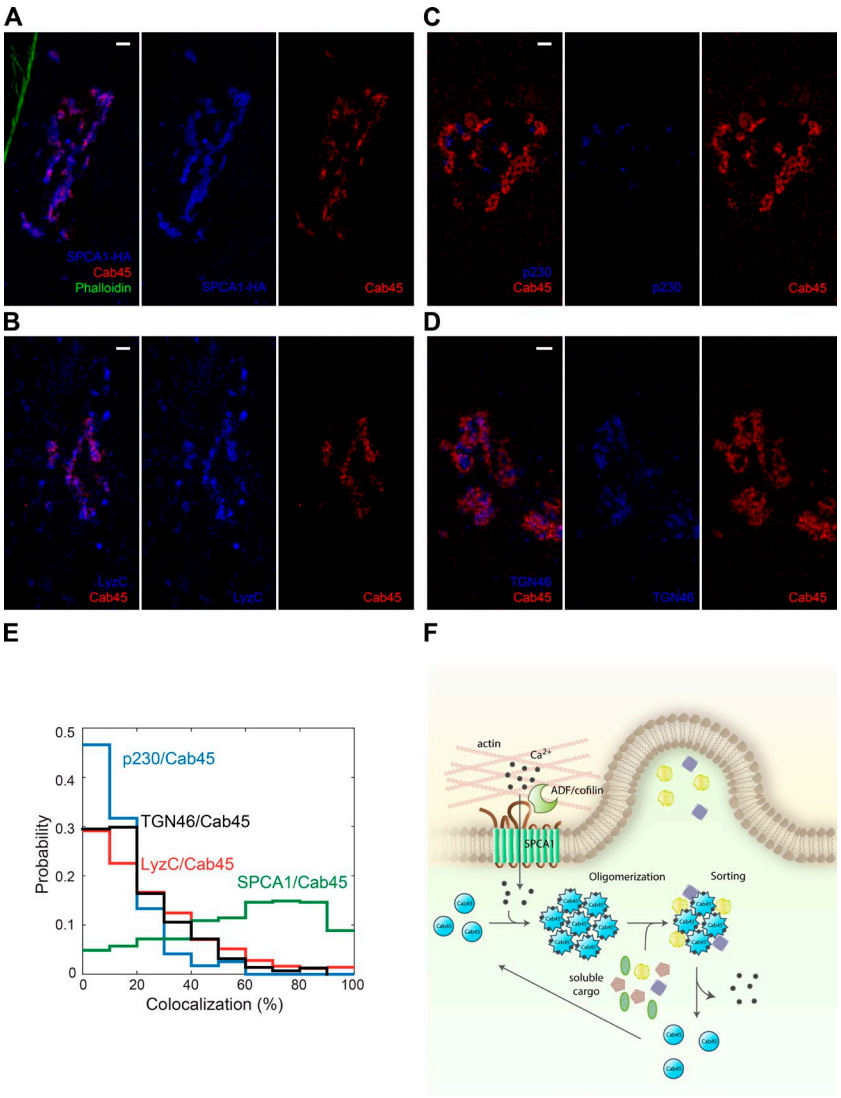

Figure 5. **SPCA1, Cab45 and cargo cluster in the TGN.** To obtain higher resolution, 3D SIM was applied. HeLa cells expressing HA-SPCA1 were fixed and stained with anti-HA and anti-Cab45 antibodies and phalloidin and analyzed by 3D SIM. (A) Representative cross section showing the locally overlapping distributions of SPCA1 and Cab45 in the TGN. Bar, 5 µm. (B) HeLa cells expressing Flag-LyzC were fixed and stained with Flag (LyzC) and Cab45 antibodies. Bar, 5 µm. (C) HeLa cells were fixed and stained with p230 and Cab45 antibodies. Bar, 5 µm. (D) HeLa cells were fixed and stained with TGN46 and Cab45 antibodies. (E) Probability (i.e., normalized frequency) of Cab45 colocalization with SPCA1, LyzC, p230, and TGN46. Depiction of the image quantification is shown in Fig. S3 (C, F, I, and L). (F) Schematic depiction of the putative Cab45-based sorting mechanism. Cab45 undergoes a conformational change upon the SPCA1-mediated local increase in Ca^{2+} concentration in the TGN lumen. As a consequence, Cab45 binds cargo proteins and separates them from other soluble proteins in the TGN by sequestering them in putative subdomains. This sorting mechanism might enable cells to pack soluble cargos into vesicles and recycle Cab45 for a new cycle of sorting by extrusion of internal Ca^{2+}.

Plasmids

The pLPCX-based plasmids used for production of full-length WT and mutant Cab45 were generated by RT-PCR from HeLa cells total RNA. The cDNA was then amplified using the primers HA-Cab45-F 5′-CGT GGATCCATGGTCTGGCCCTGGGTG-3′ and HA-Cab45-R 5′-GCA GAATTCTTAAGCGTAGTCTGGGACGTCGTATGGGTAAAACTC CTCGTGCACGCTGCG-3′ and ligated into the pLPCX backbone using BglII and EcoRI restriction sites. The Cab45 mutant was generated by inserting point mutations in EFh 1 (E122Q), EFh 2 (E161Q), EFh 3 (E220Q), EFh 4 (E257Q), EFh 5 (E302Q), and EFh 6 (E338Q).

The cDNA of SPCA1-HA was amplified with 5′-CTGGTCGAC ATGAAGGTTGCACGTTTTCAAAAAATACCTAATG-3′ and 5′-GCAGAATTCTTAAGCGTAGTCTGGGACGTCGTATGGGTATAC TTCAAGAAAAGATGATGATGTCGAACTAACATG-3′ and ligated into the pLPCX backbone using SalI and EcoRI restriction sites.

For the expression of a HIS-SUMO-tagged version of Cab45 in SF9 cells, the cDNA was amplified from the pLPCX-Cab45 (WT) plasmid with the primers 5′-CAGCGTCTCAAGGTCGGCCTGCCA ACCACTCGTC-3′ (forward) and 5′-CAGTCTAGATTAAAACTC CTCGTGCACGCTGCG-3′ (reverse) and inserted into a pI-Insect Secretory SUMOstar Vector (3106; Life Sensors). The guide RNA oligos and their complementary sequences used for CRISPR/Cas9 targeting of Cab45 were phosphorylated and annealed by a temperature gradient. Afterward, oligos were inserted into the PX459 mammalian expression vector (48139; Addgene) with BbsI restriction sites (Ran et al., 2013). Flag-LyzC in a pcDNA3.1 backbone was a gift from V. Malhotra (Centre for Genomic Regulation, Barcelona, Spain; von Blume et al., 2012).

Cell culture and stable transfection

WT HeLa cells and HeLa cells stably expressing Cab45-HA WT and Cab45-HA-6EQ-mut or SPCA1-HA, and Cab45 CRISPR KO cells (see CRISPR/Cas9 knockout cell lines section for details) were grown in DMEM (PAA) medium containing 10% FCS at 37°C with 5% CO_2. To generate cell lines stably expressing Cab45-HA WT or Cab45-HA-6EQ-mut, VSV-G pseudotyped retroviral vectors were produced by transient transfection of HEK293T cells. Viral particles were concentrated from cell culture supernatant and used for infection (Pfeifer et al., 2000).

Transient transfections

For secretion experiments, 10^7 HeLa cells were transfected with 20 µg Flag-LyzC using a TransIT-HeLaMONSTER transfection kit (Mirus) and incubated for 24 h before the secretion experiment. For Cab45 knockout, 7×10^5 HeLa cells were transfected with 4 µg of the PX459 vector encoding the sgRNA and Cas9 with the aid of the same reagent.

CRISPR/Cas9 knockout cell lines

The guide sequence of 20 nt targeting human Cab45 (also known as SDF4) was designed using the CRISPR design tool at www.genome-engineering.org/crispr (Hsu et al., 2013) and cloned into a mammalian expression vector (pX459) bearing the Cas9 coding sequence, the sequences encoding the RNA components and a puromycin selection cassette (plasmid 48139; Addgene; Ran et al., 2013). The guide sequences used to target exon 2 of human Cab45 were 5′-TTCTGATGGACGCGTCTGCA-3′ (guide 1) and 5′-TTGATGAGGACGCGGAGCCG-3′ (guide 2). A total of 4 µg of the pX459 vector containing the sequence of the sgRNA was transfected into HeLa cells. 24 h after transfection, cells were selected for 48 h in 2 µg/ml puromycin. Then, 100 cells were seeded in 15-cm culture dishes and cultured until single-cell colonies were large enough to be manually scraped off the dish and transferred to 96-well plates. Single clones were then expanded and screened for Cab45 by WB.

Generation of an anti-Cab45 antibody

For antibody generation, full-length recombinant Cab45 protein (tagged with His-Sumo; see Purification of recombinant proteins section for details) was prepared with TiterMax Gold Adjuvant liquid (Sigma-Aldrich) according to the manufacturer's protocol. Rabbits were injected and boosted three times before serum collection. Sera were incubated (while stirring) at room temperature for 1 h and then at 4°C overnight. After centrifugation for 30 min at 5,000 *g*, supernatants were collected and stored at −20°C.

Purification of recombinant proteins

His-Sumo-tagged Cab45 was expressed from the pI-secSUMOstar plasmid in SF9 cells and purified from cell supernatants by nickel-based affinity chromatography using an NaP, pH 8.0, buffer containing 500 mM NaCl and cOmplete His-tag Purification Resin (Roche). After elution with 250 mM imidazole, proteins were dialyzed against 20 mM Pipes, pH 6.8, containing 500 mM NaCl and 10% glycerol vol/vol for storage.

Protein labeling

Recombinant Cab45 and the putative cargoes COMP and CathepsinD were labeled with NHS-ATTO488 (Sigma-Aldrich) or maleimide Alexa Fluor 647 (Thermo Fisher Scientific) according to the manufacturers' instructions.

CD spectroscopy

CD measurements were performed in a 1-mm (path length) cuvette at 10°C on a JASCO J-715 spectrometer. Protein samples (0.2 mg/ml) were dissolved in 1.3 mM Pipes, pH 6.8, 33 mM NaCl, and 0.7% glycerol, and the indicated amounts of Ca^{2+} were added before spectra were recorded. A mean of 10 ($\pm Ca^{2+}$ analysis) or 4 (titration assay) independent spectra (from 195 to 250 nm with 0.1 nm spacing) were recorded. CONTIN analysis was done using CDPro. CONTIN decomposes the CD signal into six secondary structure elements: regular α-helical, distorted α-helical, regular β sheet, distorted β sheet, turn, and unordered. Reported values in the main text for the α-helical and β sheet content were the sum of regular and distorted fractions for each secondary element.

Purification of Golgi membranes

HeLa or HeLa S3 cells stably expressing Cab45-HA WT or Cab45-HA-6EQ-mut were harvested and pelleted. Pellets were then washed once in breaking buffer (BB; 10 mM Tris, pH 7.4, and 250 mM sucrose), diluted 1:5 in BB supplemented with complete Tablets Mini EDTA-free (Roche), and homogenized with a European Molecular Biology Laboratory cell cracker. After addition of 1 mM EDTA, the sucrose concentration of the homogenate was adjusted to 37% (wt/vol) and overlaid with 35% and 29% sucrose in 10 mM Tris, pH 7.4. Cellular components were separated by ultracentrifugation for 3 h at 133,000 *g*. The Golgi membrane fraction was isolated, adjusted to BB conditions, and snap-frozen in liquid nitrogen for storage at −80°C.

Analysis of the size distribution of native Cab45

Golgi membranes extracted from HeLa cells were diluted in BB and pelleted by centrifugation at 100,000 *g* for 1 h. The pellet was resuspended in 50 µl BB and incubated with DMSO or BAPTA-AM (25 µM) for 15 min at 37°C. Membranes were subsequently lysed in NativePAGE sample buffer (Thermo Fisher Scientific) supplemented with 1% DDM for 15 min and centrifuged at 20,000 *g* for 30 min at 4°C. The same protocol was followed for membranes extracted from the cell lines Cab45$^{-/-}$, Cab45$^{-/-}$ Cab45-HA WT, and Cab45$^{-/-}$ Cab45-HA 6EQ-mut. Supernatants were aliquoted into microcentrifuge tubes and stored at −80°C. Recombinant His-Sumo–tagged Cab45 was either left untreated or incubated with 1 mM Ca^{2+} or 1 mM Ca^{2+}/1 mM EGTA for 15 min on ice before electrophoresis.

NativePAGE

Golgi membranes or recombinant Cab45 were supplemented with 5% G-250 sample additive (Thermo Fisher Scientific) and loaded on a NativePAGE Novex Bis-Tris Gel (3–12%; Thermo Fisher Scientific). After transfer of the proteins onto a polyvinylidene fluoride membrane for 90 min, the membrane was immersed in 6% acetic acid for 15 min, then air-dried and washed with 100% methanol. Finally, membranes were blocked with 4% BSA in TBS for 30 min and incubated with the primary antibody overnight at 4°C.

Immunofluorescence microscopy

For immunostaining, HeLa cells were cultured on glass slides, fixed for 10 min with 4% paraformaldehyde, washed with PBS, and subsequently permeabilized for 5 min in 0.2% Triton X-100 and 0.5% SDS in 4% BSA solution. After washing again in PBS and blocking of slides for 1 h in 4% BSA, cells were incubated with the primary antibody followed with the secondary antibody, each for 1 h at room temperature. Slides were then mounted with Prolong gold antifade reagent (Thermo Fisher Scientific) and viewed at 22°C on a ZEISS confocal laser-scanning LSM 780 microscope equipped with a 40× (NA 1.4 oil) Plan-Apochromat or 100× (NA 1.46 oil) objective. For detection of Alexa Fluor, the 488-nm laser line was used. Pictures were acquired using Leica software (ZEN 2010) and processed, merged, and gamma adjusted in ImageJ (version 1.37).

Generation of a structural model of Cab45

The Cab45 structure was predicted using the Phyre2 server (Kelley and Sternberg, 2009) using the intensive mode. Six templates were chosen by the server to model human Cab45: 3q5i(A), 2f33(A), 3ek7(A), 4p5w(A), 3lij(A), and 4p60(B). The model was displayed using MacPyMOL (PyMOL Molecular Graphics System, version 1.7.4; Schrödinger, LLC). EFh (as defined in CDD entry cd00051) were assigned and predicted using SMART (Letunic et al., 2015) and CD search (Marchler-Bauer et al., 2015), and the more divergent EFh 2 was confirmed using HHPred (Söding, 2005). All EFhs were highlighted in the structure.

LyzC and COMP sorting assays

HeLa control cells and Cab45 knockout cells or cells stably expressing pLCPX-Cab45-HA WT or pLPCX-Cab45-HA 6EQ-mut, respectively, were transfected with Flag-LyzC. Cells were washed five times with serum-free medium and then grown in serum-free medium for 4 h. Cells

were then counted and lysed in PBS supplemented with 1% CHAPS. Media from each cell line were collected, clarified by passage through a 0.45-µm filter (EMD Millipore) and centrifuged at 5,000 *g* for 15 min. Samples were then concentrated using a 3 kD molecular mass cutoff spin column (EMD Millipore). Cell lysates and concentrated media were subsequently analyzed by WB using an anti-COMP or anti-Flag antibody (to detect LyzC).

Fluorescence fluctuation spectroscopy and fluorescence correlation spectroscopy

Fluorescence fluctuation spectroscopy and fluorescence correlation spectroscopy with pulsed interleaved excitation (Müller et al., 2005) were performed on a home-built confocal multiparameter fluorescence detection setup (Müller et al., 2005), which uses spectral and polarization separation in addition to fluorescence-lifetime information. The system is built around a Nikon TE2000 microscope. As picosecond excitation sources, we used an amplified frequency-doubled diode laser (PicoTA; PicoQuant) at 480 nm and a diode laser at 636 nm (LDH-P-C-635b; PicoQuant) for fluorophore excitation. Each laser is coupled into a single-mode fiber (AMS Technologies), collimated (Schäfter & Kirchhoff) and focused on the sample by a 60× 1.27 NA water-immersion objective (Plan Apo VC 60× WI; Nikon). A mean excitation power of 10 µW was used, measured at the rear aperture of the objective. A dichroic mirror (DualLine z532/635; AHF Analysentechnik) separates excitation and emission beam paths. The collected fluorescence is focused on an 80-µm pinhole (Thorlabs) via the microscope tube lens, and is passed through an emission filter (BrightLine HC 582/75; AHF Analysetechnik). Fluorescence is collected by one or more single-photon–counting avalanche photodiodes (SPQR-16; PerkinElmer) and registered by independent time-correlated single photon counting data collection cards (SPC-154; Becker & Hickl). The lasers and data collection cards are synchronized by the laser controller (Sepia; PicoQuant). For the fluorescence correlation spectroscopy measurements, labeled Cab45 was diluted to a concentration of ∼10 nM in 20 mM Pipes, pH 6.8, and 500 mM NaCl. The solutions were preincubated for 5 min before measurements were started to allow for equilibration of the sample. To calculate diffusion coefficients for Cab45 and Cab45 cargo complexes, the focus size was fixed by assuming a diffusion coefficient of 400 $\mu m^2/s$ for carboxylic acid-free ATTO488 (taken from http://www.picoquant.com/appnotes.htm). Cab45 and Cab45 cargo complexes were measured at least three times for 150 s. All experiments were performed at 22°C.

FRAP and colocalization

FRAP experiments were conducted on a spinning-disk confocal microscope system (Revolution system; Andor Technology) consisting of a base (TE2000E; Nikon) and a spinning-disk unit (CSU10; Yokogawa Electric Corporation) with a 100× oil immersion objective (NA 1.49; Nikon) at 20°C. The detection path was equipped with an Optosplit II (Cairn Research Ltd.) for dual-color detection, a filter set for EGFP and Cy5 (BS562, HC525/50, and ET605/70; AHF Analysentechnik AG), and a DU-897 Ixon EMCCD camera (Andor Technology). In addition, a triple-band dichroic beam splitter was used to separate laser excitation from fluorescence emission (Di01-T405/488/568/647; Semrock). The excitation was controlled with a tunable acousto-optic filter (Gooch & Housego). FRAP experiment were done by first acquiring five frames, then applying a bleaching pulse for 5 s and finally acquiring 300 frames. The chosen time interval between consecutive frames was between 2 s. ZEN 2010 software (ZEISS) was used for image acquisition, whereas image analysis was done with ImageM.

3D SIM

Superresolution imaging with 3D SIM was performed with a DeltaVision OMX v3 (GE Healthcare) equipped with a 100×/1.40 NA PlanApo oil immersion objective (Olympus), Cascade II:512 EMC CD cameras (Photometrics), and 405-, 488-, and 593-nm diode lasers. Samples were mounted with VECTASHIELD Mounting Medium (Vector Laboratories) and illuminated with coherent scrambled laser light directed through a movable optical grating. Image stacks with 15 images per plane (five phases, three angles) and a z-distance of 125 nm were acquired at ∼23°C and subjected to a computational reconstruction (softWoRX; Applied Precision).

3D SIM image analysis

3D SIM raw data were first reconstructed with the software softWoRx 6.0 Beta 19 (unreleased) and corrected for color shifts. A custom-made macro in Fiji (Schindelin et al., 2012) was used to establish composite TIFF stacks that are subsequently loaded as RGB into the volocity calculation software (Volocity 6.1.2; PerkinElmer). Structures were obtained, segmented, and measured in all channels by using the threshold commands "threshold using intensity" and "exclude objects by size." Reconstruction artifacts and background were also removed. Colocalizing structures were recognized by the "intersect and compartmentalize" command and quantified according to volume and number. Several small volumes belonging to one compartment were combined. Cab45 was set as 100%. Overlapping volumes were used to calculate the degree of overlap in percentage. Finally, a histogram was calculated using 10% bins.

dSTORM microscopy

To visualize Cab45 in the TGN with dSTORM, HeLa cells were incubated with Ca^{2+}/Mg^{2+}-containing HBSS (Invitrogen) supplemented with 2 g/l glucose, 490 µM $MgCl_2$, and 450 µM $MgSO_4$; 300 mOsmol/l, pH 7.4, and DMSO or the same buffer without Ca^{2+} containing 2 µM ionomycin and 5 mM EGTA (Palmer and Tsien, 2006) and incubated for 10 min. Then, cells were fixed as described in the Immunofluorescence microscopy section and stained with an anti-Cab45 primary and a Cy5-labeled secondary antibody. Before performing dSTORM imaging, a glucose oxidase-based oxygen scavenging buffer was added according to a slightly modified version of the protocol described in (Dempsey et al., 2011). Imaging buffer contained 100 mM mercaptoethylamine (Fluka) as a reducing agent, 2.5% (wt/vol) glucose (Sigma-Aldrich), 0.5 mg/ml glucose oxidase (Sigma-Aldrich), and 3 µl/ml catalase suspension (concentration ∼20–50 mg/ml; Sigma-Aldrich). dSTORM imaging (Heilemann et al., 2008) was performed at room temperature (22°C) on a combined wide-field/total internal reflection fluorescence microscope described previously (Prescher et al., 2015) using a home-built microscope stage in combination with a SR Apo total internal reflection fluorescence 100× oil objective (Nikon) with a numerical aperture of 1.49. Images were detected by an EMCCD camera (DU860D-CS0-BV; Andor Technology) using Solis software (version 4.19.3; Andor Technology).

For each dSTORM image, a movie stack comprising 10,000 frames at a frame rate of 20 Hz was acquired using wide-field illumination. Cy5 fluorophores were excited at a wavelength of λ_{exc} = 642 nm and a laser power of 50 mW, which was measured at the output of the objective. In some cases, additional activation was required, which was realized by changing the imaging mode to activation cycles, where each cycle consisted of one activation frame (λ_{exc} = 488 nm), followed by nine imaging frames (λ_{exc} = 642 nm). Laser power for imaging was kept at 50 mW, whereas the power of the activating laser was gradually increased from 0 to ∼2 mW over the course of data acquisition.

dSTORM image analysis

Rendering and analysis of the acquired dSTORM images was performed using a home-written software created with MATLAB R2014b (The MathWorks) as described elsewhere (Prescher et al., 2015). In brief, a 2D Gaussian function was fitted to the detected point-spread functions using Levenberg-Marquard's nonlinear least squares algorithm. Sample drift was corrected by pixel-wise cross-correlation of each frame of the image stack with the first frame of this stack. As demonstrated previously (Bates et al., 2007), image drift can then be obtained by tracking of the centroid position of the correlation function. A polynomial fit was applied to the obtained drift function to reduce fluctuations caused by fluorophore blinking. For rendering of the final high-resolution image, each localized molecule was displayed by a 2D Gaussian function with a fixed amplitude of 1,000 counts and a standard deviation corresponding to the respective image resolution, which was derived from the localization accuracy and was on average 39 ± 8 nm. Events that appeared in two or more consecutive frames within a distance <1 px (120 nm) were considered as originating from the same fluorescent molecule. Localized molecules with <300 detected photons were discarded. Further, all molecules with an ellipticity $E = |(\sigma_x - \sigma_y)/(\sigma_x + \sigma_y)| > 15\%$ were discarded for the control cells as well as all events with $E > 50\%$ for the ionomycin-treated cells.

Statistical analysis

Statistical significance was analyzed in an unpaired Student's *t* test using GraphPad Prism software. Compared datasets were statistically significant when p-values were <0.01 (**).

Online supplemental material

Fig. S1 shows by STROM microscopy that the TGN remains intact in ionomycin treated cells. In addition, cargo clustering by Cab45 and Ca^{2+} and fluorescence cross-correlation spectroscopy experiments show that only the Ca^{2+} bound form of Cab45 binds cargo. In Fig. S2, we show control experiments for the Cab45 CRSIPR/Cas9 cell lines (immunofluorescence and secretion assays). Fig. S3 visualizes different quantification images from 3D SIM images depicted in Fig. 5. Online supplemental material is available at http://www.jcb.org/cgi/content/full/jcb.201601089/DC1.

Acknowledgments

We thank H. Reiter for retroviral transfections. We thank W. Neupert and M. Harner for insightful discussions. We thank S. Suppmann from the Max Planck Institute biochemistry core facility for Cab45 expression and purification.

The group of J. von Blume is funded by an Emmy Noether Fellowship (project BL 1186/1-1), by Deutsche Forschungsgemeinschaft CRC914 (TP A09), and by an FP7 Marie Curie Career Reintegration Grant. J. von Blume is supported by the Max Planck Institute of Biochemistry and by the department of Molecular Medicine of Reinhard Fässler. The group of D.C. Lamb is grateful for financial support from the Deutsche Forschungsgemeinschaft through SFB1035 (project A11) and the Center for NanoScience Munich. D.C. Lamb and H. Leonhardt are supported by the Excellence Clusters Nanosystems Initiative Munich and Center for integrated Protein Science Munich.

The authors declare no competing financial interests.

Submitted: 25 January 2016
Accepted: 6 April 2016

References

Aulestia, F.J., M.T. Alonso, and J. García-Sancho. 2015. Differential calcium handling by the cis and trans regions of the Golgi apparatus. *Biochem. J.* 466:455–465. http://dx.doi.org/10.1042/BJ20141358

Bates, M., B. Huang, G.T. Dempsey, and X. Zhuang. 2007. Multicolor super-resolution imaging with photo-switchable fluorescent probes. *Science.* 317:1749–1753. http://dx.doi.org/10.1126/science.1146598

Bonifacino, J.S. 2014. Adaptor proteins involved in polarized sorting. *J. Cell Biol.* 204:7–17. http://dx.doi.org/10.1083/jcb.201310021

Cardoso, M.C., K. Schneider, R.M. Martin, and H. Leonhardt. 2012. Structure, function and dynamics of nuclear subcompartments. *Curr. Opin. Cell Biol.* 24:79–85. http://dx.doi.org/10.1016/j.ceb.2011.12.009

Cong, L., F.A. Ran, D. Cox, S. Lin, R. Barretto, N. Habib, P.D. Hsu, X. Wu, W. Jiang, L.A. Marraffini, and F. Zhang. 2013. Multiplex genome engineering using CRISPR/Cas systems. *Science.* 339:819–823. http://dx.doi.org/10.1126/science.1231143

Curwin, A.J., J. von Blume, and V. Malhotra. 2012. Cofilin-mediated sorting and export of specific cargo from the Golgi apparatus in yeast. *Mol. Biol. Cell.* 23:2327–2338. http://dx.doi.org/10.1091/mbc.E11-09-0826

De Matteis, M.A., and A. Luini. 2008. Exiting the Golgi complex. *Nat. Rev. Mol. Cell Biol.* 9:273–284. http://dx.doi.org/10.1038/nrm2378

Dempsey, G.T., J.C. Vaughan, K.H. Chen, M. Bates, and X. Zhuang. 2011. Evaluation of fluorophores for optimal performance in localization-based super-resolution imaging. *Nat. Methods.* 8:1027–1036. http://dx.doi.org/10.1038/nmeth.1768

Doray, B., K. Bruns, P. Ghosh, and S. Kornfeld. 2002. Interaction of the cation-dependent mannose 6-phosphate receptor with GGA proteins. *J. Biol. Chem.* 277:18477–18482. http://dx.doi.org/10.1074/jbc.M201879200

Fölsch, H., H. Ohno, J.S. Bonifacino, and I. Mellman. 1999. A novel clathrin adaptor complex mediates basolateral targeting in polarized epithelial cells. *Cell.* 99:189–198. http://dx.doi.org/10.1016/S0092-8674(00)81650-5

Fölsch, H., M. Pypaert, P. Schu, and I. Mellman. 2001. Distribution and function of AP-1 clathrin adaptor complexes in polarized epithelial cells. *J. Cell Biol.* 152:595–606. http://dx.doi.org/10.1083/jcb.152.3.595

Guo, Y., D.W. Sirkis, and R. Schekman. 2014. Protein sorting at the trans-Golgi network. *Annu. Rev. Cell Dev. Biol.* 30:169–206. http://dx.doi.org/10.1146/annurev-cellbio-100913-013012

Heilemann, M., S. van de Linde, M. Schüttpelz, R. Kasper, B. Seefeldt, A. Mukherjee, P. Tinnefeld, and M. Sauer. 2008. Subdiffraction-resolution fluorescence imaging with conventional fluorescent probes. *Angew. Chem. Int. Ed. Engl.* 47:6172–6176. http://dx.doi.org/10.1002/anie.200802376

Hsu, P.D., D.A. Scott, J.A. Weinstein, F.A. Ran, S. Konermann, V. Agarwala, Y. Li, E.J. Fine, X. Wu, O. Shalem, et al. 2013. DNA targeting specificity of RNA-guided Cas9 nucleases. *Nat. Biotechnol.* 31:827–832. http://dx.doi.org/10.1038/nbt.2647

Kelley, L.A., and M.J.E. Sternberg. 2009. Protein structure prediction on the Web: a case study using the Phyre server. *Nat. Protoc.* 4:363–371. http://dx.doi.org/10.1038/nprot.2009.2

Kienzle, C., and J. von Blume. 2014. Secretory cargo sorting at the trans-Golgi network. *Trends Cell Biol.* 24:584–593. http://dx.doi.org/10.1016/j.tcb.2014.04.007

Kienzle, C., N. Basnet, A.H. Crevenna, G. Beck, B. Habermann, N. Mizuno, and J. von Blume. 2014. Cofilin recruits F-actin to SPCA1 and promotes Ca2+-mediated secretory cargo sorting. *J. Cell Biol.* 206:635–654. http://dx.doi.org/10.1083/jcb.201311052

Kornfeld, S., and I. Mellman. 1989. The biogenesis of lysosomes. *Annu. Rev. Cell Biol.* 5:483–525. http://dx.doi.org/10.1146/annurev.cb.05.110189.002411

Letunic, I., T. Doerks, and P. Bork. 2015. SMART: recent updates, new developments and status in 2015. *Nucleic Acids Res.* 43:D257–D260. http://dx.doi.org/10.1093/nar/gku949

Lissandron, V., P. Podini, P. Pizzo, and T. Pozzan. 2010. Unique characteristics of Ca^{2+} homeostasis of the trans-Golgi compartment. *Proc. Natl. Acad. Sci. USA.* 107:9198–9203. http://dx.doi.org/10.1073/pnas.1004702107

Marchler-Bauer, A., M.K. Derbyshire, N.R. Gonzales, S. Lu, F. Chitsaz, L.Y. Geer, R.C. Geer, J. He, M. Gwadz, D.I. Hurwitz, et al. 2015. CDD: NCBI's conserved domain database. *Nucleic Acids Res.* 43:D222–D226. http://dx.doi.org/10.1093/nar/gku1221

Meissner, G. 1975. Isolation and characterization of two types of sarcoplasmic reticulum vesicles. *Biochim. Biophys. Acta.* 389:51–68. http://dx.doi.org/10.1016/0005-2736(75)90385-5

Mellman, I., and W.J. Nelson. 2008. Coordinated protein sorting, targeting and distribution in polarized cells. *Nat. Rev. Mol. Cell Biol.* 9:833–845. http://dx.doi.org/10.1038/nrm2525

Missiaen, L., K. Van Acker, K. Van Baelen, L. Raeymaekers, F. Wuytack, J.B. Parys, H. De Smedt, J. Vanoevelen, L. Dode, R. Rizzuto, and G. Callewaert. 2004. Calcium release from the Golgi apparatus and the endoplasmic reticulum in HeLa cells stably expressing targeted aequorin to these compartments. *Cell Calcium.* 36:479–487. http://dx.doi.org/10.1016/j.ceca.2004.04.007

Müller, B.K., E. Zaychikov, C. Bräuchle, and D.C. Lamb. 2005. Pulsed interleaved excitation. *Biophys. J.* 89:3508–3522. http://dx.doi.org/10.1529/biophysj.105.064766

Palade, G. 1975. Intracellular aspects of the process of protein synthesis. *Science.* 189:867. http://dx.doi.org/10.1126/science.189.4206.867-b

Palmer, A.E., and R.Y. Tsien. 2006. Measuring calcium signaling using genetically targetable fluorescent indicators. *Nat. Protoc.* 1:1057–1065. http://dx.doi.org/10.1038/nprot.2006.172

Pfeifer, A., T. Kessler, S. Silletti, D.A. Cheresh, and I.M. Verma. 2000. Suppression of angiogenesis by lentiviral delivery of PEX, a noncatalytic fragment of matrix metalloproteinase 2. *Proc. Natl. Acad. Sci. USA.* 97:12227–12232. http://dx.doi.org/10.1073/pnas.220399597

Pizzo, P., V. Lissandron, P. Capitanio, and T. Pozzan. 2011. Ca^{2+} signalling in the Golgi apparatus. *Cell Calcium.* 50:184–192. http://dx.doi.org/10.1016/j.ceca.2011.01.006

Prescher, J., V. Baumgärtel, S. Ivanchenko, A.A. Torrano, C. Bräuchle, B. Müller, and D.C. Lamb. 2015. Super-resolution imaging of ESCRT-proteins at HIV-1 assembly sites. *PLoS Pathog.* 11:e1004677. http://dx.doi.org/10.1371/journal.ppat.1004677

Ran, F.A., P.D. Hsu, J. Wright, V. Agarwala, D.A. Scott, and F. Zhang. 2013. Genome engineering using the CRISPR-Cas9 system. *Nat. Protoc.* 8:2281–2308. http://dx.doi.org/10.1038/nprot.2013.143

Schermelleh, L., R. Heintzmann, and H. Leonhardt. 2010. A guide to super-resolution fluorescence microscopy. *J. Cell Biol.* 190:165–175. http://dx.doi.org/10.1083/jcb.201002018

Schindelin, J., I. Arganda-Carreras, E. Frise, V. Kaynig, M. Longair, T. Pietzsch, S. Preibisch, C. Rueden, S. Saalfeld, B. Schmid, et al. 2012. Fiji: an open-source platform for biological-image analysis. *Nat. Methods.* 9:676–682. http://dx.doi.org/10.1038/nmeth.2019

Söding, J. 2005. Protein homology detection by HMM-HMM comparison. *Bioinformatics.* 21:951–960. http://dx.doi.org/10.1093/bioinformatics/bti125

Tagliabracci, V.S., J.L. Engel, J. Wen, S.E. Wiley, C.A. Worby, L.N. Kinch, J. Xiao, N.V. Grishin, and J.E. Dixon. 2012. Secreted kinase phosphorylates extracellular proteins that regulate biomineralization. *Science.* 336:1150–1153. http://dx.doi.org/10.1126/science.1217817

Traub, L.M., and S. Kornfeld. 1997. The trans-Golgi network: a late secretory sorting station. *Curr. Opin. Cell Biol.* 9:527–533. http://dx.doi.org/10.1016/S0955-0674(97)80029-4

von Blume, J., J.M. Duran, E. Forlanelli, A.-M. Alleaume, M. Egorov, R. Polishchuk, H. Molina, and V. Malhotra. 2009. Actin remodeling by ADF/cofilin is required for cargo sorting at the trans-Golgi network. *J. Cell Biol.* 187:1055–1069. http://dx.doi.org/10.1083/jcb.200908040

von Blume, J., A.-M. Alleaume, G. Cantero-Recasens, A. Curwin, A. Carreras-Sureda, T. Zimmermann, J. van Galen, Y. Wakana, M.A. Valverde, and V. Malhotra. 2011. ADF/cofilin regulates secretory cargo sorting at the TGN via the Ca^{2+} ATPase SPCA1. *Dev. Cell.* 20:652–662. http://dx.doi.org/10.1016/j.devcel.2011.03.014

von Blume, J., A.-M. Alleaume, C. Kienzle, A. Carreras-Sureda, M. Valverde, and V. Malhotra. 2012. Cab45 is required for Ca^{2+}-dependent secretory cargo sorting at the trans-Golgi network. *J. Cell Biol.* 199:1057–1066. http://dx.doi.org/10.1083/jcb.201207180

Wiech, H., B.M. Geier, T. Paschke, A. Spang, K. Grein, J. Steinkötter, M. Melkonian, and E. Schiebel. 1996. Characterization of green alga, yeast, and human centrins. Specific subdomain features determine functional diversity. *J. Biol. Chem.* 271:22453–22461. http://dx.doi.org/10.1074/jbc.271.37.22453